Journal of Inflammation Research

Dovepress
Taylor & Francis Group

Open Access Full Text Article

ORIGINAL RESEARCH

Elucidating the Mechanism of Fusu Agent Against Sepsis-Induced Acute Respiratory Distress Syndrome via an Integrated Approach Combining Network Pharmacology, Molecular Dynamics Simulations, and Experimental Validation

Ni Jin[1], Xiangting Wang[1], Mei Lai[1], Jiaxi Zou[1,2], Liying He[3], Gan Luo[4], Xiujuan Zhou[2], Peiyang Gao[2]

[1]Department of Clinical Medical, Chengdu University of Traditional Chinese Medicine, Chengdu, Sichuan, People's Republic of China; [2]Department of Critical Care Medicine, Hospital of Chengdu University of Traditional Chinese Medicine, Chengdu, Sichuan, People's Republic of China; [3]Department of TCM Regulating Metabolic Diseases Key Laboratory of Sichuan Province, Hospital of Chengdu University of Traditional Chinese Medicine, Chengdu, Sichuan, People's Republic of China; [4]Department of Animal & Veterinary Sciences, Southwest Minzu University, Chengdu, Sichuan, People's Republic of China

Correspondence: Peiyang Gao; Xiujuan Zhou, Email gaopy930@126.com; zhouxiujuan@cdutcm.edu.cn

Background: Sepsis represents a critical medical condition that frequently progresses to acute respiratory distress syndrome (ARDS). While the traditional Chinese medicine Fusu agent (FSHJ) is clinically effective, its precise mechanisms in sepsis-induced ARDS remain unclear.

Methods: To elucidate the therapeutic mechanisms of FSHJ in sepsis-induced ARDS, we implemented an integrated multi-method strategy combining network pharmacology, molecular dynamics simulations (MDS), liquid chromatography-mass spectrometry (LC-MS), and in vivo validation. Active compounds and targets of FSHJ were identified from Batman-TCM 2.0, followed by protein–protein interaction network construction via STRING. Kyoto Encyclopedia of Genes and Genomes (KEGG) and Gene Ontology (GO) enrichment analyses were performed using clusterProfiler in R. Molecular docking with AutoDock Vina assessed binding affinities, and MDS with GROMACS verified complex stability. LC-MS confirmed the predicted bioactive components, while animal models experimentally validated the associated signaling pathways.

Results: A total of 537 shared therapeutic targets were pinpointed among FSHJ, ARDS, and sepsis. Integrative assessments of protein–protein interaction (PPI) networks along with GO and KEGG enrichment analyses highlighted that the anti-sepsis-induced ARDS activity of FSHJ is predominantly mediated through inflammatory response regulation. Docking simulations combined with molecular dynamics analyses demonstrated that the key bioactive compound quercetin exhibited robust and sustained interactions with specific protein targets. LC-MS analyses further authenticated the presence of anticipated active compounds, particularly the glycoside derivative quercetin-3β-D-glucoside. Furthermore, all three doses of FSHJ effectively alleviated pathological lung tissue damage and systemic inflammatory responses induced by *Escherichia coli* (*E. coli*) infection. Relative to the control (model) group, FSHJ markedly suppressed the mRNA expression of inflammatory cytokines *IL-6, IL-1β*, and *TNF-α*, and decreased protein expression levels of TLR4 and NF-κB p65.

Conclusion: Our findings indicate that FSHJ exerts protective effects in an *E. coli*-induced sepsis-associated ARDS mouse model, potentially through the regulation of TLR4/NF-κB-mediated inflammatory signaling pathways.

Keywords: Fusu agent, acute respiratory distress syndrome, sepsis, network pharmacology, molecular dynamics simulations, *Escherichia coli* (*E. coli*)

https://doi.org/10.2147/JIR.S572866
Received: 3 November 2025
Accepted: 4 March 2026
Published: 25 March 2026

Graphical Abstract

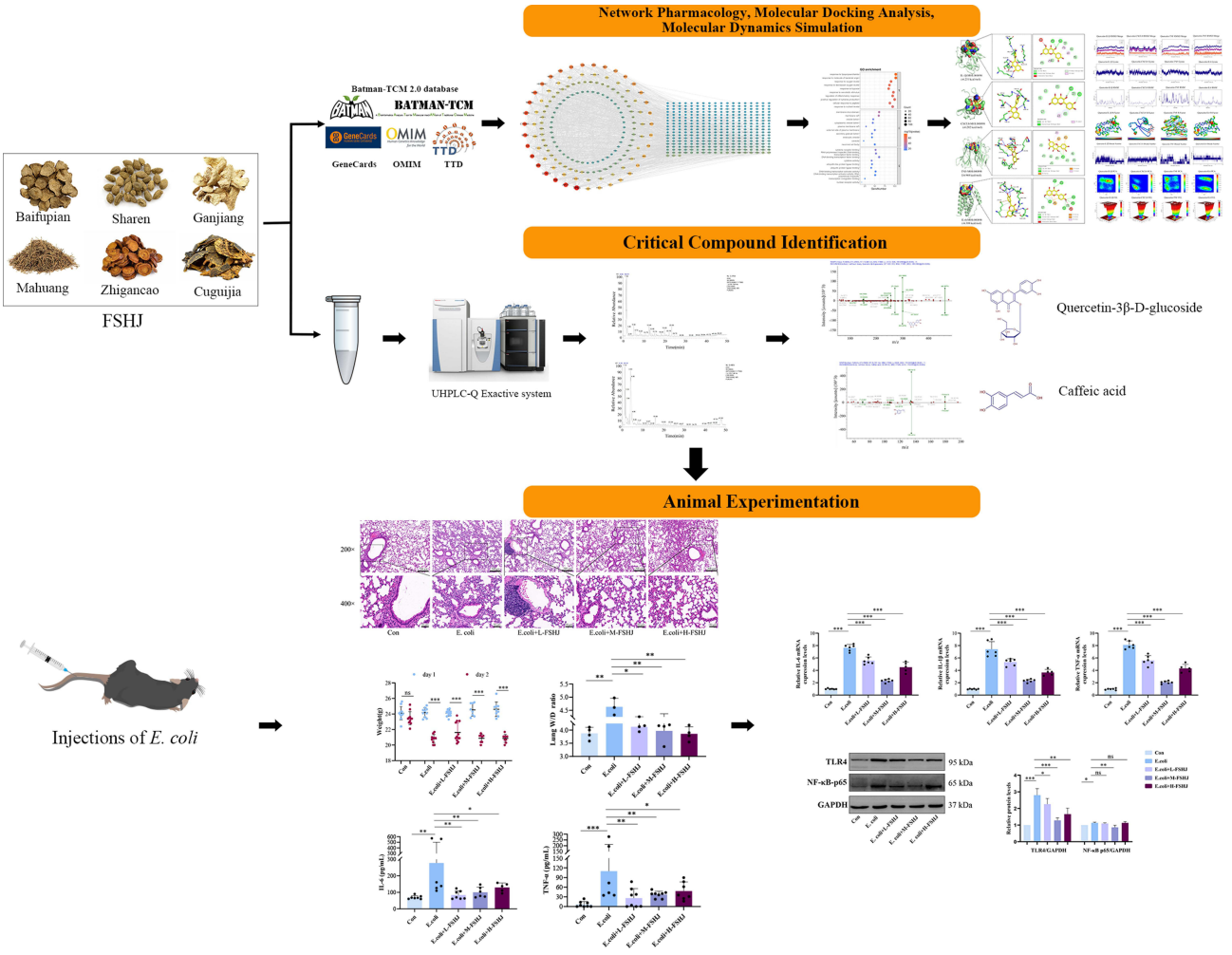

Introduction

Sepsis is an acute medical syndrome characterized by organ dysfunction resulting from an unregulated immune response triggered by infection.[1] Pulmonary tissue often exhibits high susceptibility in sepsis scenarios, initially presenting as acute lung injury (ALI) which can escalate progressively into acute respiratory distress syndrome (ARDS).[2] Reports indicate that the incidence of ALI/ARDS approaches 41%, with ARDS significantly contributing to elevated sepsis-related mortality (34–45%).[3–5] ALI/ARDS involves acute respiratory impairment characterized by enhanced alveolar-capillary barrier permeability, resulting in pulmonary inflammation, hypoxemia, and edema.[6–8] Present therapeutic interventions largely emphasize symptomatic relief and supportive care; nonetheless, patient outcomes remain inadequate due to the absence of efficacious pharmacological treatments.[9–11] Consequently, identifying novel therapeutic options and elucidating the pathological mechanisms underlying sepsis-induced ARDS is of critical importance.

Traditional Chinese medicine (TCM) has been extensively utilized for therapeutic purposes over centuries. Recent literature highlights how TCM modulates inflammatory processes and macrophage polarization in ALI/ARDS.[12,13] Chinese herbal medicines and their active constituents typically feature multiple targets, multiple pathways, and minimal adverse effects.[14] Notably, the holistic principles of TCM align closely with the multi-target therapeutic strategy required for managing ARDS pathogenesis and progression.[13] The Fusu agent (Fusuheji, FSHJ), inspired by the Qianyang Dan

formula from the Qing Dynasty, is a TCM prescription formulated according to TCM theory. It includes *Aconiti Lateralis Radix Praeparata* (Baifupian), *Amomum villosum Lour* (Sharen), *Zingiberis Rhizoma* (Ganjiang), *Ephedra Herba* (Mahuang), *Radix Glycyrrhizae Preparata* (Zhigancao), and *Testudinis Carapax et Plastrum* (Cuguijia). In our previous multicenter prospective randomized controlled trial, FSHJ significantly reduced 28-day and 90-day mortality rates in ARDS patients and improved the PaO_2/FiO_2 ratio.[15] Furthermore, animal studies demonstrated that FSHJ protected against lipopolysaccharide (LPS)-induced ALI in rats by repairing endothelial barrier function.[16] Nevertheless, the underlying molecular mechanisms of FSHJ in sepsis-induced ARDS require further exploration.

Network pharmacology represents a systematic analytical framework enabling comprehensive assessment of drug-disease interactions, facilitating mechanistic insights at the molecular level.[17,18] Structure-based molecular docking serves as a computational approach to predict and analyze the interactions between bioactive compounds and their potential target proteins.[19] The current investigation combines network pharmacology, docking simulations, molecular dynamics analyses (MDS), and in vivo experiments to identify potential molecular targets and mechanistic pathways by which FSHJ alleviates sepsis-induced ARDS. The findings from this comprehensive analysis furnish essential scientific foundations for subsequent clinical investigations.

Materials and Methods

Identification of Active Ingredients and Molecular Targets of FSHJ

Potential molecular targets for the primary ingredients (Baifupian, Sharen, Ganjiang, Mahuang, Zhigancao, and Cuguijia) were identified using the Batman-TCM 2.0 database.[20] The search source was set to "known targets only", with the following filter criteria: "Adjusted P-value cutoff to 0.05" and "Druggable Score $\geq$ 0.9". Duplicate targets were subsequently removed, resulting in a refined and unique set of molecular targets linked to the active ingredients of FSHJ.

Screening of Potential Targets for Sepsis-Induced ARDS and Active Compounds of FSHJ

Potential therapeutic targets for sepsis-induced ARDS were systematically retrieved from three public databases: GeneCards, OMIM, and TTD. Searches utilized the keywords "Acute Respiratory Distress Syndrome" and "Sepsis". Duplicates were removed, yielding a consolidated list of disease-related targets. The intersection of disease targets and FSHJ active ingredient targets was determined through Venn diagram analysis to identify potential key therapeutic targets.

Construction and Topological Analysis of Herbal Compound–Target–Disease Network

Connections between FSHJ, active ingredients, corresponding targets, and sepsis-induced ARDS were organized in Excel. The relationships were visualized and analyzed using Cytoscape (v3.8.2). Topological parameters were employed to identify the network's core elements.

Construction of Protein–Protein Interaction (PPI) Network and Identification of Core Targets

A PPI network was generated using overlapping targets between FSHJ and sepsis-induced ARDS from the STRING database, restricting results to *Homo sapiens* with default parameters. Network visualizations and corresponding data in TSV format were exported for subsequent analytical procedures. Cytoscape (version 3.8.2) facilitated the topological analysis, which involved calculating degree, betweenness centrality, and closeness centrality. The Maximal Clique Centrality (MCC) algorithm was applied to identify the ten most critical core targets.

Enrichment Analysis

Utilizing the R package clusterProfiler, we conducted enrichment studies to determine the functional relevance of shared targets, taking into account Kyoto encyclopedia of genes and genomes (KEGG) and gene ontology (GO) pathways. We

ranked the terms by significance, selected those with an adjusted P-value < 0.05, and sorted this subset in ascending order of P-value. Ten of the most important GO keywords and twenty of the most important KEGG pathways were visualized.

Molecular Docking

We used the MCC algorithm rankings from the PPI network to choose the top 10 candidate therapeutic compounds and the top 10 target proteins for molecular docking. Compounds' three-dimensional structures (in SDF format) were obtained from PubChem. The RCSB Protein Data Bank was utilized for the extraction of protein crystal structures. Molecular docking evaluations were carried out using AutoDock Vina, and docking affinities were meticulously documented. Complexes with a binding affinity of ≤ −5.0 kcal/mol were defined as stably bound.

Trajectory Analysis for Structural Stability

Using the GROMACS 2022 program, MDS were executed. The General Amber Force Field was used to parameterize ligands, while the AMBER ff14SB force field was used for proteins. Using TIP3P water molecules and periodic boundary conditions, systems were solvated. Under the control of the V-rescale thermostat and the Berendsen barostat, the simulation circumstances comprised an NPT ensemble operating at 298 K and 1 bar. A 2-fs timestep was made possible by limiting bond lengths using the LINCS method. The Particle Mesh Ewald (PME) technique terminated non-bonded interactions at 1.0 nm and computed long-range electrostatic interactions with a cutoff of 1.2 nm. At each of the ten steps, the neighbor lists were updated. During the equilibration process, the NVT ensemble was used for 100 ps first, and the NPT ensemble for 100 ps second. The simulations for the production phase were run for 100 ns, and every 10 ps, we took a snapshot of the trajectory to analyze with VMD and PyMOL.

Liquid Chromatography-Mass Spectrometry (LC-MS) and Animal Experiments

Drug Preparation

FSHJ was formulated from six authenticated medicinal materials: Baifupian, Cuguijia, Sharen, Ganjiang, Zhigancao, and Mahuang, in a dry-weight ratio of 6:4:3:3:2:2. Herbs were obtained from the Pharmacy of the Hospital of Chengdu University of TCM and met quality standards outlined in the Chinese Pharmacopoeia (2020 edition).

FSHJ was prepared following the standardized protocols outlined in the Regulations on Decoction for Medical Institutions in China. Specifically, the herbal components were initially immersed in purified water, ensuring the water level remained approximately 2–5 cm above the herb surface. The mixture was then heated until boiling, after which it was maintained at a gentle simmer for 40–60 minutes. Subsequently, the decoction underwent filtration to separate the liquid extract, while the residual herbal material was subjected to a second extraction step with fresh purified water. Both resulting filtrates were combined, concentrated under reduced pressure at a temperature of 70 °C until the relative density reached 1.2, and subsequently freeze-dried for 72 hours at −70 °C. The lyophilized material was then finely ground into powder, sealed into airtight bags, and stored at −20 °C pending further experimentation.

Culture and Preparation of Escherichia Coli (E. Coli)

After inoculating 100 mL of LB broth with one *E. coli* colony, the mixture was cultured overnight at 180 rpm for about 12–16 hours. To prepare the bacteria for experimentation, they were centrifuged at 5000 rpm for 10 minutes after cultivation. The pelleted bacteria were then resuspended in sterile PBS, reaching a concentration of 2×10^9 CFU/mL.

LC-MS Analysis

The FSHJ samples were first subjected to ultrasonic extraction in a 3:1 v/v ratio of methanol and water, and then filtered through a 0.22-μm membrane filter. Thermo Fisher Scientific's UHPLC-Q Exactive apparatus was used for subsequent analysis of the filtrates. The Accucore™ C18 column, which was kept at 40 °C, was used for chromatographic separation. At a flow rate of 0.40 mL/min, with injection quantities of 5 μL, the mobile phase was composed of acetonitrile (solvent A) and 0.1% formic acid (solvent B). Using both positive and negative ionization modes, mass spectrometric detection was carried out across a m/z range of 100–1500.

Animals and Experimental Design

Approval No.: 2024DL-034 from the Affiliated Hospital of Chengdu University of Traditional Chinese Medicine's Ethics Committee allowed the conduct of animal studies in accordance with established protocols. Using a 12-hour light-dark cycle, male C57BL/6 mice were housed in a specified pathogen-free (SPF) environment. The mice were procured from the Sipeifu Company in Beijing. The mice were given free reign to eat and drink anything the lab staff deemed appropriate.

Sixty mice were randomly assigned to five experimental groups using a random number generator (see Table S1): Control (Con, n = 11), *E. coli* group (n = 13, 2×10^8 CFU), low-dose FSHJ (L-FSHJ, n = 12, 1.59 g/kg/day), medium-dose FSHJ (M-FSHJ, n = 12, 3.18 g/kg/day), and high-dose FSHJ (H-FSHJ, n = 12, 6.36 g/kg/day). These three FSHJ doses were based on the human equivalent dose (HED). The HED (1.59 g/kg/day) was calculated from the clinical dose (10.5 g/day for a 60 kg adult) using a conversion factor of 9.1. The medium and high doses were set at two and four times the HED, respectively.

Sepsis models were established via intravenous tail vein injection of *E. coli* ATCC 25922 (2×10^8 CFU per mouse, Testobio, Ningbo, Lot No. TS275207).[21,22] During bacterial injection, one mouse from the model group and one from the H-FSHJ group were excluded due to technical failure of tail vein injection. Drug treatments began 3 h after infection, with a second dose administered 24 h later.[23] Prior to the experimental endpoint, further mortality was observed: two mice in the model group, one in the M-FSHJ group, and two in the H-FSHJ group died and were therefore excluded from the final analysis. Consequently, a total of 53 mice were included in the study.

Mice in the FSHJ-treated groups received 300 μL of respective formulations twice via oral gavage, while control and *E. coli* groups received equal volumes of saline. All animals were euthanized 36 hours post-infection by intraperitoneal injection of sodium pentobarbital (60 mg/kg). Body weights were recorded immediately before sampling.

Histopathological Examination by Hematoxylin and Eosin (H&E) Staining

Lung tissues were fixed using 4% paraformaldehyde, subjected to routine dehydration procedures, and embedded into paraffin blocks. Sections (4-μm thickness) obtained from these paraffin-embedded tissues were subsequently deparaffinized using xylene and stained with H&E. After completing dehydration and clearing processes, sections were mounted with neutral gum and observed under a light microscope for histopathological evaluation.

Evaluation of Pulmonary Edema by Lung Wet-to-Dry (W/D) Weight Ratio

Wet weight was determined by promptly weighing the surgically resected right middle lobe of the lung after meticulous blotting to remove excess fluid. After that, the tissues were heated at 60 °C in an oven until they reached a consistent dry weight. Pulmonary edema was diagnosed by calculating the W/D weight ratio.

Enzyme-Linked Immunosorbent Assay (ELISA)

Serum levels of IL-6 and TNF-α in mice were measured using ELISA kits obtained from Elabscience (Wuhan, China; IL-6 kit: E-EL-M0044, TNF-α kit: E-EL-M3063).

RNA Extraction and Quantitative Real-Time PCR (qRT-PCR)

Lung tissues from mice were processed to extract total RNA using the Animal Total RNA Isolation Kit (Cat. No. RE-03014). The AccuRT Genomic DNA Removal Kit (ABM, Jiangsu, China; Cat. No. G492) and 5× All-In-One MasterMix were used to do complementary DNA synthesis. A real-time PCR apparatus was used to conduct qRT-PCR with EvaGreen Express 2× qPCR MasterMix-No Dye (ABM; Cat. No. MasterMix-ES). A denaturation step of 5 minutes at 95 °C was preceded by 40 amplification cycles of 10 seconds at 95 °C and 30 seconds at 60 °C as part of the PCR amplification protocol. The examination of the melting curve showed a temperature range of 60–95 °C, with 0.3 °C increments every 15 seconds. We used the $2^{-\Delta\Delta CT}$ calculation method to quantify gene expression levels after normalizing them to *β-actin* (Table 1).

Western Blot (WB)

In order to homogenize the lung tissue samples from mice, phosphatase inhibitors were added to the RIPA lysis buffer. The supernatants containing total protein extracts were obtained after centrifugation at 12,000 g for 10 minutes at 4 °C. After

Table 1 Primer Sequences Used in This Study

Gene	Primer	Sequence (5'-3')
β-Actin	Forward	GTGCTATGTTGCTCTAGACTTCG
	Reverse	ATGCCACAGGATTCCATACC
IL-6	Forward	CTGCAAGAGACTTCCATCCAG
	Reverse	AGTGGTATAGACAGGTCTGTTGG
IL-1β	Forward	GAAATGCCACCTTTTGACAGTG
	Reverse	TGGATGCTCTCATCAGGACAG
TNF-α	Forward	CAGGCGGTGCCTATGTCTC
	Reverse	CGATCACCCCGAAGTTCAGTAG

adjusting the sample quantities to guarantee uniformity, the protein concentrations were measured using a BCA assay kit. After transferring proteins to PVDF membranes, SDS-PAGE was used to resolve them. After that, the proteins were blocked with 5% skim milk for 1 hour. The membranes were incubated at 4 °C overnight with primary antibodies against TLR4, NF-κB p65, and GAPDH, supplied by Proteintech, Affinity, and Servicebio, respectively (GB11519, AF7021, and 10745-1-AP, respectively). The next step was to incubate the membranes for 1 hour with secondary antibodies that were coupled to HRP. A chemiluminescent imaging system (Clinx; Shanghai, China; ChemiScope 6100) was used to detect protein bands, and the intensities of these bands were assessed using the accompanying analysis software.

Statistical Analysis Methods

Data are presented as mean ± standard deviation (SD). For statistical evaluation, GraphPad Prism version 8 software was employed. Comparisons were analyzed using independent-sample t-tests, or one-way analysis of variance (ANOVA), complemented by Fisher's LSD post-hoc tests for further examination. Statistical significance was established at a threshold of $P < 0.05$.

Results

Identification of Potential Drug and Disease Targets

FSHJ comprises several medicinal components: Baifupian, Sharen, Ganjiang, Mahuang, Zhigancao, and Cuguijia. Using predefined screening criteria, 256 drug components and 1047 targets were identified from the Batman-TCM 2.0 database. Queries with keywords "Acute respiratory distress syndrome" and "Sepsis" in the GeneCards, OMIM, and TTD databases yielded 6394 and 4193 disease-related targets, respectively. Intersection analysis identified 537 overlapping targets between FSHJ components and disease targets (Figure 1).

Component–Target–Disease Network Construction and Analysis of FSHJ

An "active ingredient–target" interaction network was generated utilizing Cytoscape version 3.8.2 software. Essential components within the network were distinguished based on critical parameters. The network diagram employed different colors to depict nodes: targets were indicated in green, active components in purple, TCM in red, and disease states in blue (Figure 2). ADME parameters predicted by SwissADME indicated that core components possess favorable pharmacokinetic properties with bioavailability greater than 0.55 (Table 2 and Table S2). Within this network, quercetin, luteolin, morphine, and 3β-hydroxyurs-12-en-28-syre exhibited a higher number of connections, suggesting their critical roles as key active ingredients of FSHJ against sepsis-induced ARDS (Figure 2).

Construction and Analysis of PPI Network

Potential targets were input into the STRING database to generate a PPI network (Figure 3a). Using the MCC algorithm, the top ten targets were identified: IL1B, CXCL8, TNF, IL6, IL1A, IL10, CSF2, IFNG, CSF3, and CXCL10 (Figure 3b). These findings suggest that these targets are critical nodes in the network and key mediators of the therapeutic effects of FSHJ on sepsis-induced ARDS.

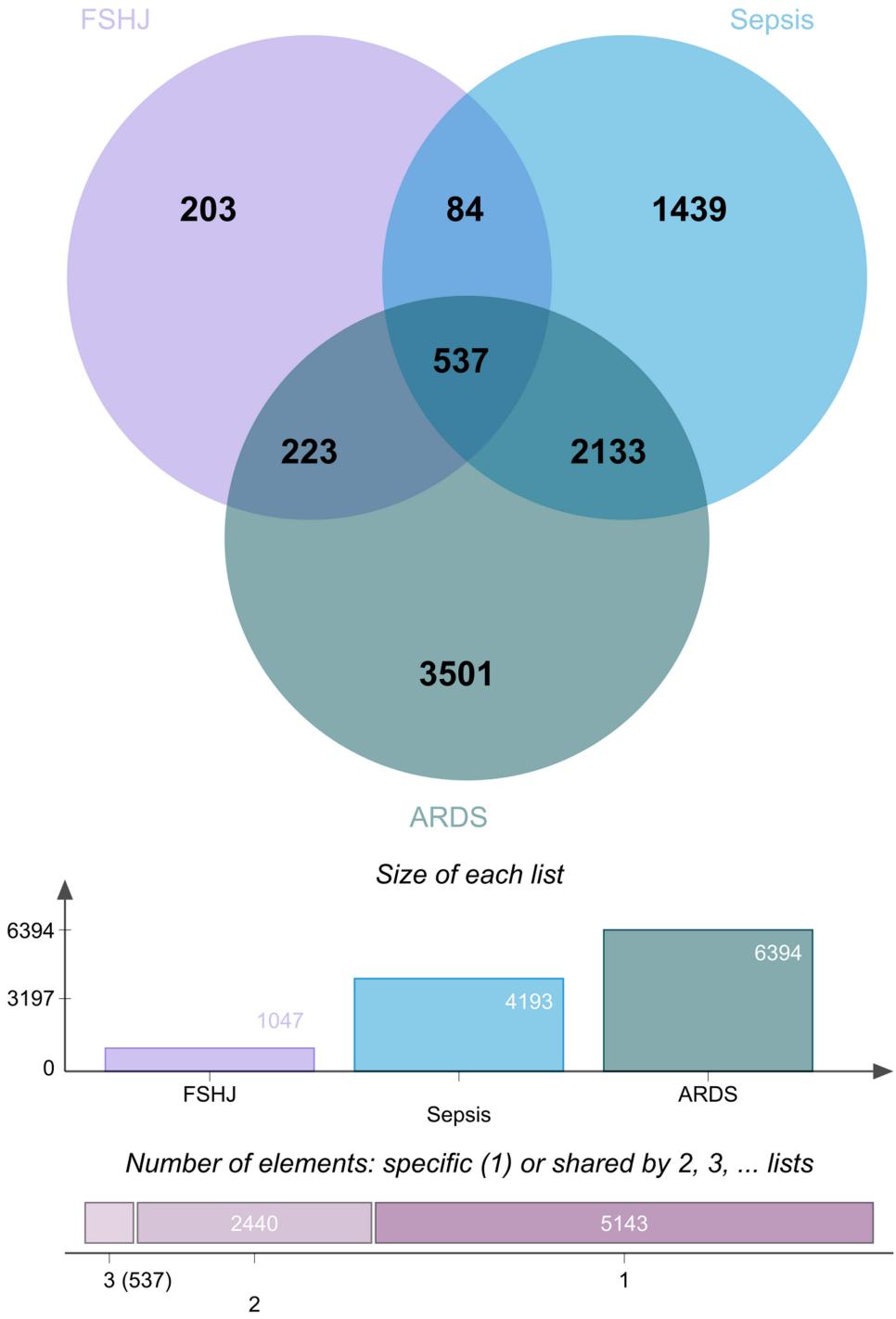

Figure 1 Venn diagram of drug active ingredient targets and disease targets.

GO/KEGG Analysis

GO enrichment analysis identified 3817 biological processes, 170 cellular components, and 306 molecular functions significantly associated with identified targets. Prominent enriched biological processes encompassed responses to lipopolysaccharide, responses to bacterial-derived molecules, and modulation of inflammatory reactions (Figure 4a). Notably, the highest enrichment scores were observed for the first two processes, closely correlating with the regulatory effects of FSHJ. Correspondingly, the mouse model in subsequent validation experiments utilized tail vein injection of *E. coli*, effectively simulating these biological responses. Additionally, KEGG analysis identified 208 pathways,

https://doi.org/10.2147/JIR.S572866

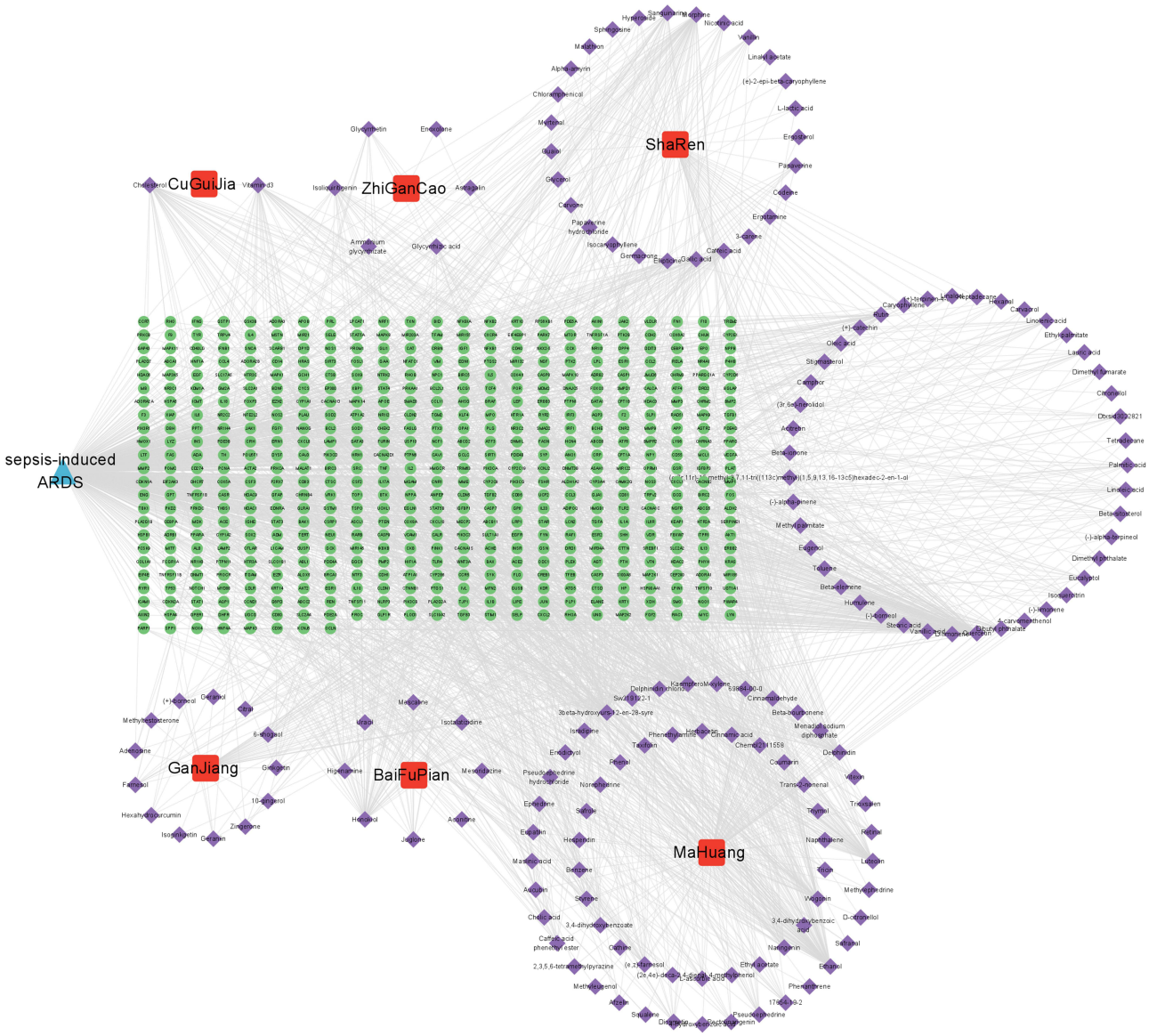

Figure 2 Component-target-disease network of FSHJ.

prominently including inflammation-related pathways: PI3K-Akt signaling pathway, major identified signaling pathways included Toll-like receptor (TLR), TNF, and IL-17 signaling pathways (Figure 4b). These collective findings suggest that inflammatory responses elicited by *E. coli* infection substantially contribute to the anti-inflammatory and protective actions of FSHJ within pulmonary tissue.

Molecular Docking

Structure-based molecular docking analyses demonstrated that quercetin exhibited strong binding affinities (below −5.0 kcal/mol) toward four critical protein targets: IL-1β, CXCL8, TNF, and IL-6 (Figures 5a–d). Quercetin formed stable complexes within the active sites of these proteins, supporting their potential as therapeutic targets.

MDS Analysis

Following the molecular docking analysis, MDS was subsequently conducted to assess the dynamic stability of interactions between quercetin and protein targets. The simulations revealed that root mean square deviation (RMSD)

Table 2 Top ten FSHJ Components Identified From the Component–Target–Disease Network

Drug	Molecule Name	Mol ID	Degree	Betweenness Centrality	Closeness Centrality	Bioavailability Score
Sharen, Ganjiang, Mahuang	Quercetin	MOL000098	165	0.060334444	0.432250153	0.55
Mahuang	Luteolin	MOL000006	65	0.00960614	0.378828587	0.55
Sharen	Morphine	MOL006979	60	0.009085463	0.370467683	0.55
Mahuang	3β-hydroxyurs-12-en -28-syre	MOL000511	60	0.008982701	0.374005305	0.55
Baifupian	Honokiol	MOL005955	57	0.007827918	0.363214838	0.55
Mahuang	Wogonin	MOL000173	49	0.005741758	0.370857443	0.55
Mahuang	Kaempferol	MOL000422	49	0.006330151	0.370467683	0.55
Cuguijia	Cholesterol	MOL000953	44	0.004283618	0.343065693	0.55
Cuguijia	Vitamin d3	MOL010861	41	0.004339106	0.347119645	0.55
Mahuang	Delphinidin	MOL004798	40	0.004314109	0.364718055	0.55

reached equilibrium over the 100 ns simulation period, signifying stable molecular conformations (Figure 6a). Additionally, radius of gyration (Rg) values exhibited minor oscillations but overall remained constant, confirming structural compactness (Figure 6b). Analysis of the root mean square fluctuation (RMSF) and B-factors revealed low flexibility in residues near the quercetin-binding sites, reinforcing binding stability (Figures 6c and d). Additionally, hydrogen bond counts fluctuated consistently between 1 and 5, indicating stable electrostatic interactions (Figure 6e).

Principal component analysis (PCA) and free energy landscape (FEL) calculations were performed to further assess stability. PCA displayed a highly populated region (red patch), indicating the most stable conformational states (Figure 6f). The FEL analysis revealed a single low-energy basin, confirming the structural stability of quercetin–protein complexes (Figure 6g). Collectively, these results confirmed that quercetin forms stable complexes with key protein targets.

Validation of Active Compounds, Therapeutic Efficacy, and Targeting Mechanisms of FSHJ

Identification of Active Compounds in FSHJ by LC-MS

LC-MS was conducted to identify active components in FSHJ. The total ion chromatograms (Figures 7a and b) revealed 25 compounds meeting inclusion criteria (Table S3). Among these, five compounds (caffeic acid, tetramethylpyrazine, catechin, afzelin, and aconitine) appeared in the Component–Target–Disease Network with a degree ≥ 2 (Table S2). However, the critical compound quercetin was not directly identified. Upon re-examining LC-MS data, quercetin-3β-D-glucoside, a quercetin derivative, was identified (Figure 7c). Thus, quercetin-3β-D-glucoside may significantly contribute to mitigating sepsis-induced ARDS. Additionally, caffeic acid was identified as another potential active component despite its lower initial ranking (Figure 7d and Tables S2–S3).

FSHJ Effectively Attenuates Lung Injury and Pulmonary Inflammation Induced by E. Coli Infection

To evaluate the protective effects of FSHJ, a mouse sepsis-induced ARDS model was established via tail-vein injection of 2×10^8 CFU of *E. coli* (Figure 8a). FSHJ treatment was initiated 3 h post-infection, and samples were collected after 36 h. Compared to pre-injection levels, all groups, except controls, showed significant body-weight reduction ($P < 0.001$, Figure 8b). The low-dose FSHJ group experienced less weight loss compared to other treatment groups (Figure 8b). Lung histopathology using H&E staining showed that *E. coli* administration caused thickened alveolar walls, inflammatory infiltration, bronchial epithelial degeneration, and alveolar capillary congestion. FSHJ treatment markedly reduced these pathological changes (Figure 8c).

Pulmonary edema severity was determined using lung W/D weight ratios. Compared to control animals, the *E. coli*-infected group exhibited significantly elevated W/D ratios indicative of edema. Administration of FSHJ markedly reduced lung edema (Figure 8d; $P < 0.05$).

https://doi.org/10.2147/JIR.S572866

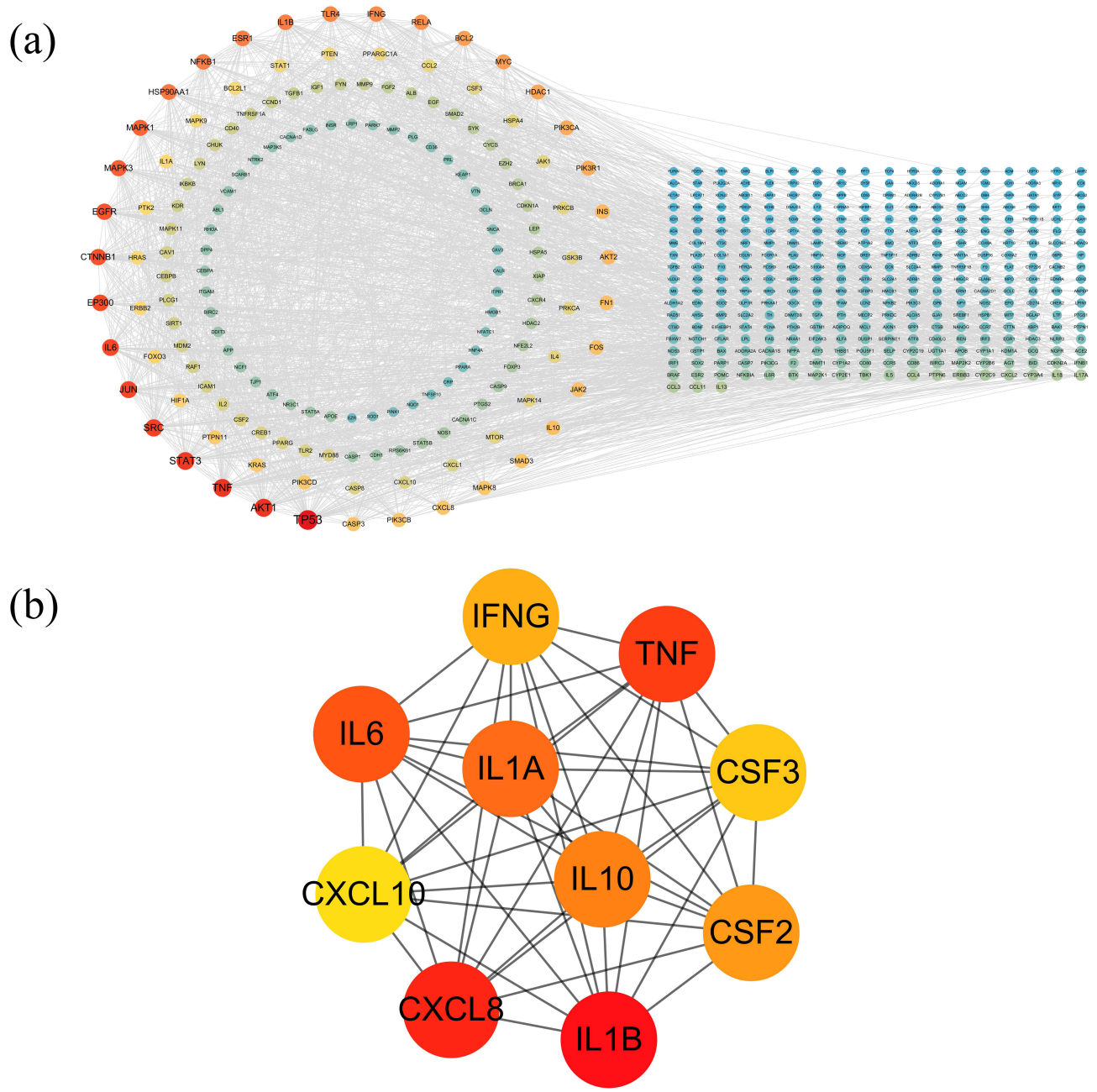

Figure 3 PPI network of therapeutic targets for FSHJ. (**a**) Complete PPI network illustrating interactions among therapeutic targets. (**b**) PPI network highlighting the top 10 targets by degree value. Colors from red to Orange represent decreasing degree values.

Additionally, ELISA assays revealed significantly diminished serum IL-6 and TNF-α concentrations following FSHJ treatment, compared to untreated *E. coli*-infected mice (Figures 8e and f; $P < 0.05$). These data robustly demonstrate the protective effect of FSHJ against sepsis-induced ARDS.

FSHJ Modulates Inflammatory Pathways in Murine Lung Tissue

To further explore the underlying anti-inflammatory mechanisms of FSHJ, lung tissue mRNA expression levels of *IL-6, TNF-α*, and *IL-1β* were assessed using quantitative RT-PCR. Results showed a pronounced decrease in these inflammatory mediators following FSHJ administration compared to the *E. coli*-infected group (Figures 9a–c; $P < 0.001$). WB analyses indicated increased expression of TLR4 and NF-κB p65 proteins in response to *E. coli* infection; however, FSHJ

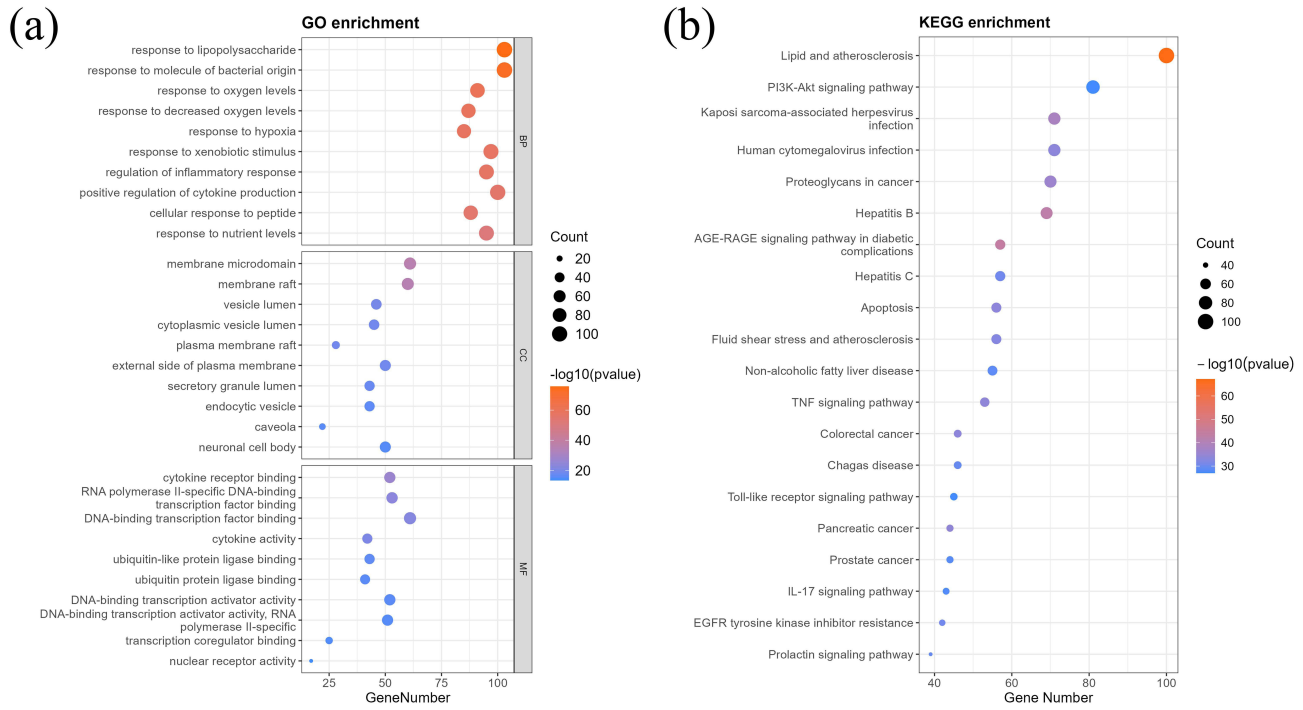

Figure 4 GO and KEGG enrichment analyses. (**a**) Top 10 GO enrichment terms. (**b**) Top 20 enriched KEGG pathways.

treatment notably reduced their expression levels (Figures 9d and e). Although NF-κB p65 protein expression changes did not consistently achieve statistical significance across all tested concentrations, a clear regulatory trend was observed.

Discussion

Sepsis-induced ARDS is a prevalent critical condition associated with a high mortality rate; however, effective targeted therapies remain lacking.[5] Thus, exploring novel therapeutic agents and clarifying their mechanisms of action are essential. TCM demonstrates significant potential in managing pulmonary diseases.[24,25] Although TCM does not specifically classify sepsis-induced ARDS, its clinical manifestations, such as hypoxemia and respiratory distress, align closely with TCM conditions.[13,26] Several TCM preparations, including Xuebijing, Shenfu Injection, and Tanreqing, exhibit beneficial effects on sepsis-induced ARDS.[17,25,27]

The FSHJ is a TCM compound preparation previously validated for clinical efficacy and protective effects in LPS-induced ALI rat models.[15,16] However, its molecular mechanisms remain unclear. In this study, the Batman-TCM 2.0 database identified 256 drug components and 1047 targets, including 537 overlapping targets between FSHJ and disease conditions. The top five core components included quercetin, luteolin, morphine, 3β-hydroxyurs-12-en-28-syre, and honokiol. Prior studies indicated these active components could mitigate ALI/ARDS by modulating inflammation and oxidative stress.[12,28–32] Additionally, wogonin and kaempferol exhibit similar effects.[33,34] LC-MS analysis also identified quercetin-3β-D-glucoside and afzelin, glycoside derivatives of quercetin and kaempferol, respectively, suggesting their potential importance in the protective action of FSHJ against sepsis-induced ARDS.

A single bacterial strain introduced via tail vein injection is optimal for sepsis modeling, eliminating confounding polymicrobial effects and accurately replicating clinical symptoms.[21] Other studies often used intraperitoneal injection of *E. coli* to establish sepsis models.[22,35–38] Thus, *E. coli* injection is widely accepted as effective for modeling sepsis. In this study, H&E staining showed thickened alveolar walls, inflammatory infiltration, bronchial epithelial cell degeneration, capillary congestion, and an increased W/D ratio after *E. coli* administration, indicating lung injury (Figures 8c and d). Additionally, *E. coli*-treated mice showed significant body weight loss and elevated serum IL-6 and TNF-α levels, suggesting systemic inflammation (Figures 8b, e and f). Comparing histopathological and inflammatory indicators across

https://doi.org/10.2147/JIR.S572866

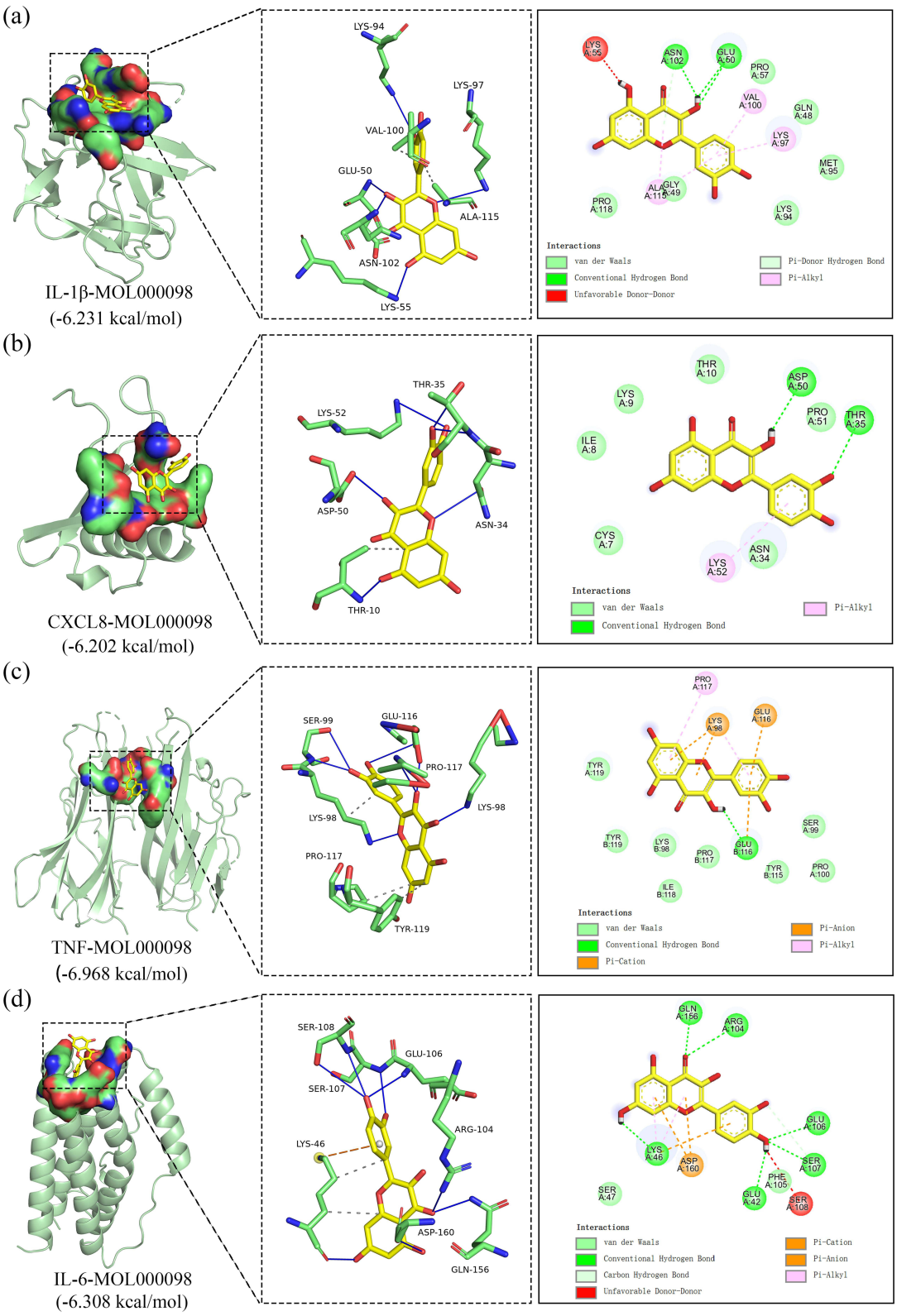

Figure 5 Molecular docking analyses (2D and 3D) of quercetin with predicted protein targets. (**a**) Quercetin docked with IL-1β. (**b**) Quercetin docked with CXCL8. (**c**) Quercetin docked with TNF. (**d**) Quercetin docked with IL-6.

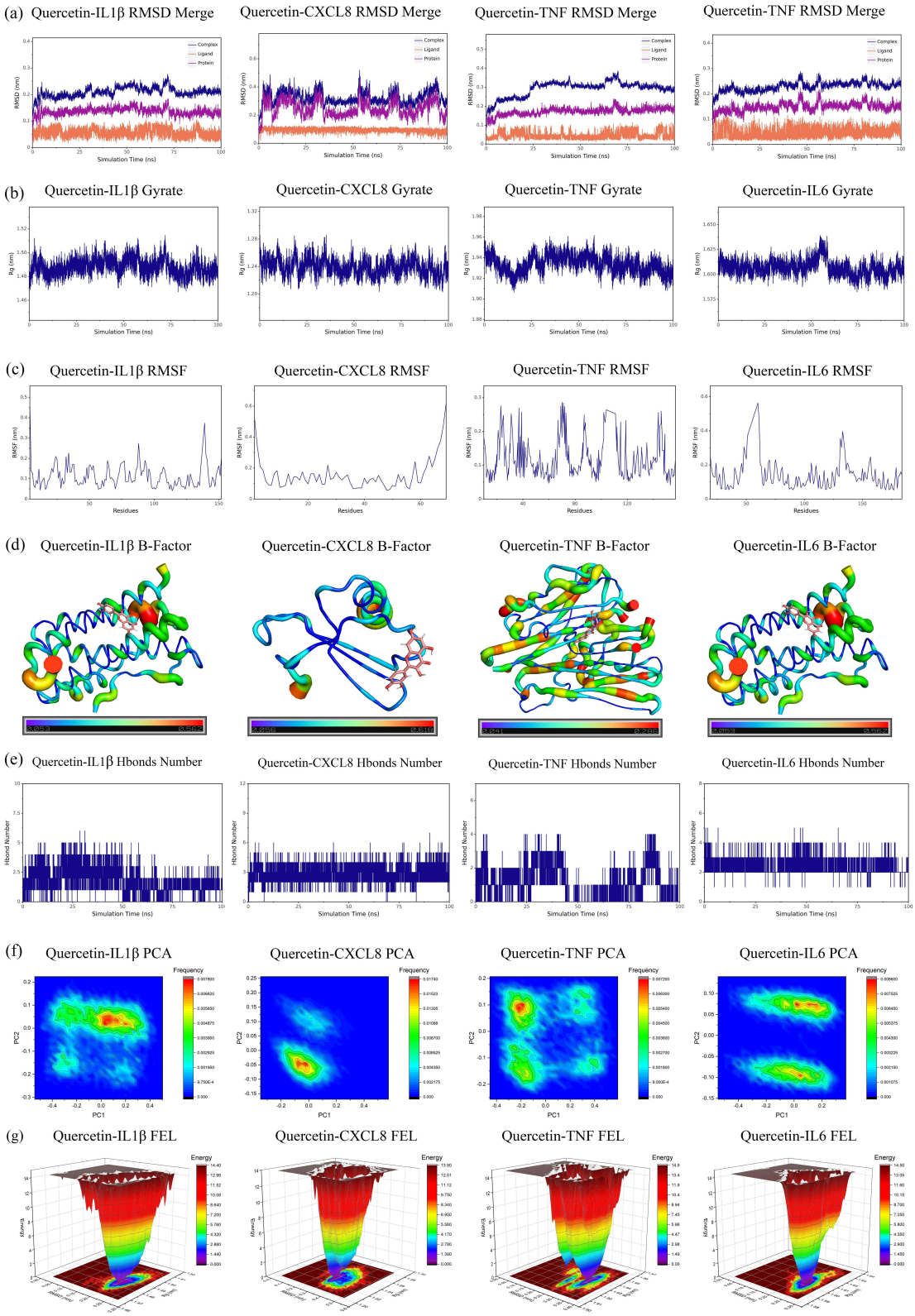

Figure 6 MDS of quercetin–protein complexes. (**a**) RMSD values for quercetin–target protein complexes. (**b**) Rg curves of protein–quercetin complexes. (**c**) RMSF profiles of proteins complexed with quercetin. (**d**) B-factor analyses of protein–quercetin complexes. (**e**) Number of hydrogen bonds formed over time. (**f**) PCA of protein–quercetin complexes. (**g**) FEL analyses of protein–quercetin complexes. RMSD: reflects the similarity between two molecular conformations; lower values indicate closer structural alignment, and stabilization over time suggests equilibrated dynamics. Rg: measures the overall compactness of the protein–ligand complex; a smaller Rg corresponds to a more compact structure, while a larger Rg implies greater structural looseness. FEL: constructed using RMSD and Rg as reaction coordinates, depicting possible conformational states and their relative stability for the complex.

https://doi.org/10.2147/JIR.S572866

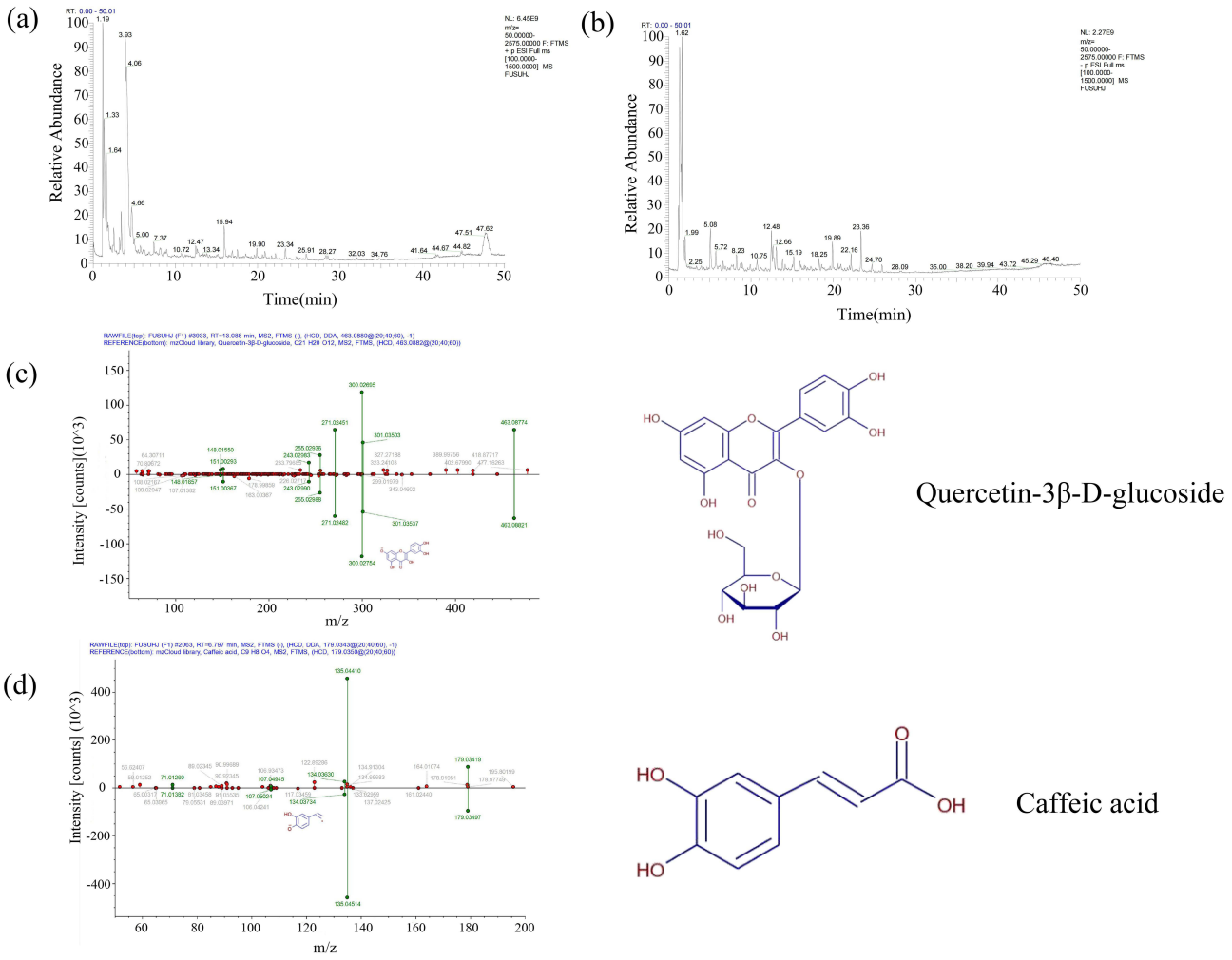

Figure 7 LC-MS total ion chromatograms and primary active compounds identified in FSHJ. (**a**) Total ion chromatogram (positive ion mode). (**b**) Total ion chromatogram (negative ion mode). (**c** and **d**) Representative main active compounds identified by LC-MS.

groups confirmed that FSHJ exhibited clear anti-inflammatory and lung-protective effects in the *E. coli*-induced lung injury model.

Integrated analysis of PPI, GO, and KEGG results clarified potential mechanisms underlying FSHJ's effects on sepsis-induced ARDS. The top ten PPI-identified targets closely related to inflammatory response (Figure 3b), consistent with GO and KEGG analyses highlighting inflammation-related pathways (Figures 4a and b). These results strongly indicate inflammatory regulation as a critical mechanism of FSHJ's therapeutic effects.

The pathogenesis of sepsis-induced ARDS is complex, involving inflammatory responses, oxidative stress, cellular infiltration, and vascular leakage.[39] Dysregulated inflammation is particularly central to ALI/ARDS development.[13,40] This inflammatory cascade damages pulmonary epithelium and endothelium, exacerbating lung injury.[7] TLRs play crucial roles in pathogen recognition and immune response initiation by detecting pathogen- or damage-associated molecular patterns.[41] Gram-negative bacteria, particularly *E. coli*, possess LPS, which is specifically recognized by TLR4, triggering downstream activation of NF-κB signaling.[42,43] Following activation, NF-κB p65 translocates to the nucleus, driving transcriptional activation and increasing pro-inflammatory cytokine expression.[40] Prior studies have illustrated that *E. coli* infection activates innate immune responses predominantly via TLR2/TLR4-mediated pathways, subsequently engaging NLRP3 inflammasome components and stimulating MAPK and NF-κB signaling cascades.[44] Corroborating these findings, our experimental data revealed elevated protein levels of TLR4 and NF-κB p65 and increased mRNA expression of *IL-6, TNF-α*, and *IL-1β* after exposure to *E. coli* (Figure 9). Remarkably, FSHJ

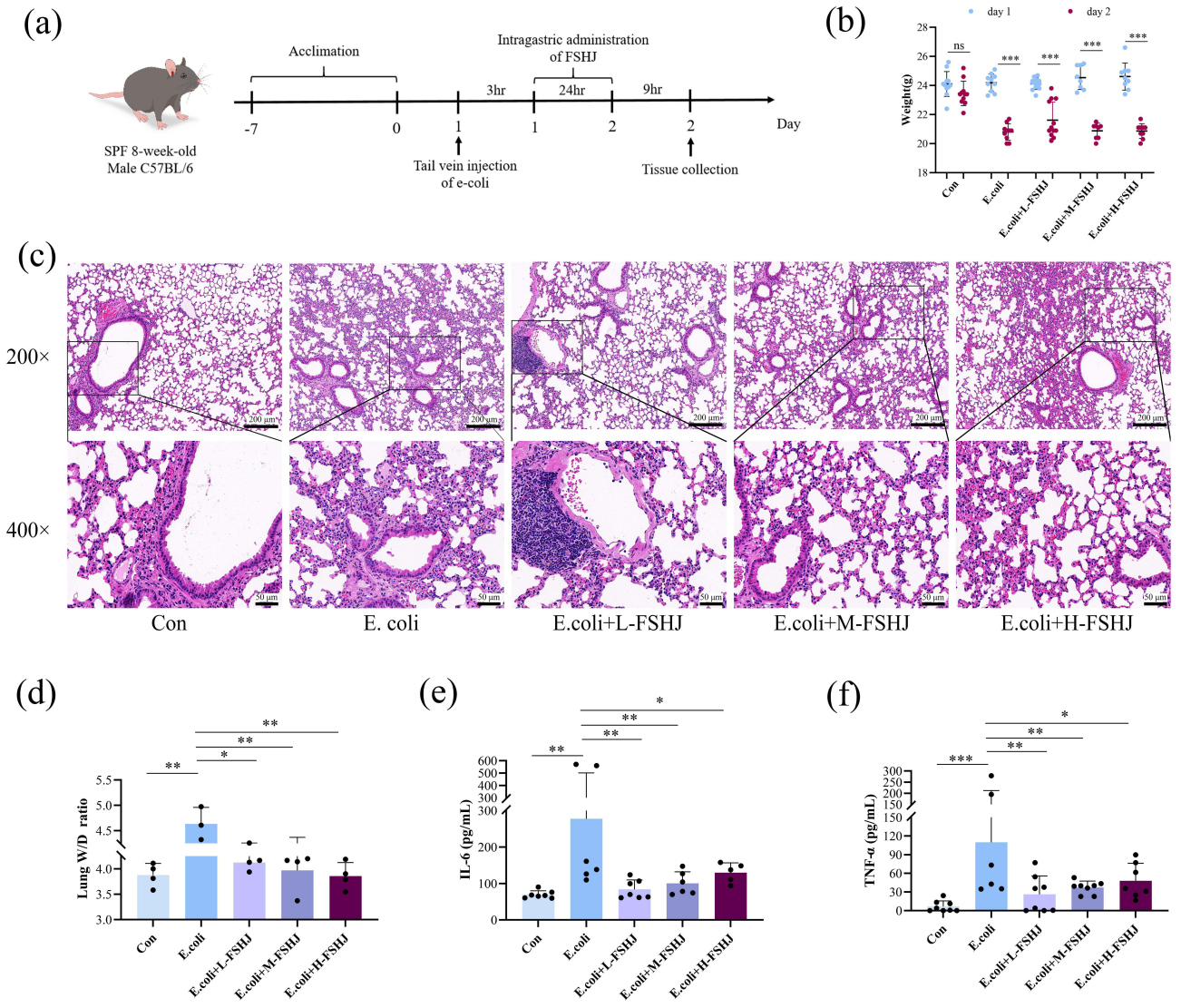

Figure 8 Protective effects of FSHJ against *E. coli*-induced ARDS in vivo. (**a**) Schematic overview of FSHJ administration protocol. (**b**) Body-weight changes in mice (n=9–12). (**c**) Histological analysis of lung tissue by H&E staining. (**d**) Lung W/D weight ratio (n=3–4). (**e** and **f**) Plasma levels of cytokines (IL-6 and TNF-α) measured by ELISA (n=5–8). **P* < 0.05, ***P* < 0.01, ****P* < 0.001. (**b**) was compared using independent-sample t-tests; (**d–f**) were compared using one-way ANOVA with Fisher's LSD post hoc test.
Abbreviation: ns, not significant.

administration reversed these inflammatory parameters, suggesting that this therapeutic effect may be mediated by the regulation of the TLR4/NF-κB pathway (Figure 9).

To validate key inflammatory targets identified through network pharmacology within the TLR4/NF-κB pathway, quercetin, the primary active ingredient in FSHJ, was selected. Molecular docking and dynamic simulations confirmed a strong and stable interaction between quercetin and the inflammatory targets.While computational analyses identified quercetin as a major active component, LC-MS further confirmed the presence of its derivative, quercetin-3β-D-glucoside, which may serve as a potential key bioactive substance mediating the therapeutic effects of FSHJ against sepsis-induced ARDS. It is noteworthy that FSHJ did not show a clear dose-response relationship, a phenomenon documented in previous studies, likely attributable to its complex composition.[45] Optimal therapeutic effects occurred at medium doses (twofold the HED).

This study has several limitations. First, our proposed mechanism involving the TLR4/NF-κB pathway requires further validation. Specifically, cellular-level evidence and interventional studies using specific pathway inhibitors are needed to establish causality. Second, the in vivo observation period was relatively short; longer-term studies are

https://doi.org/10.2147/JIR.S572866

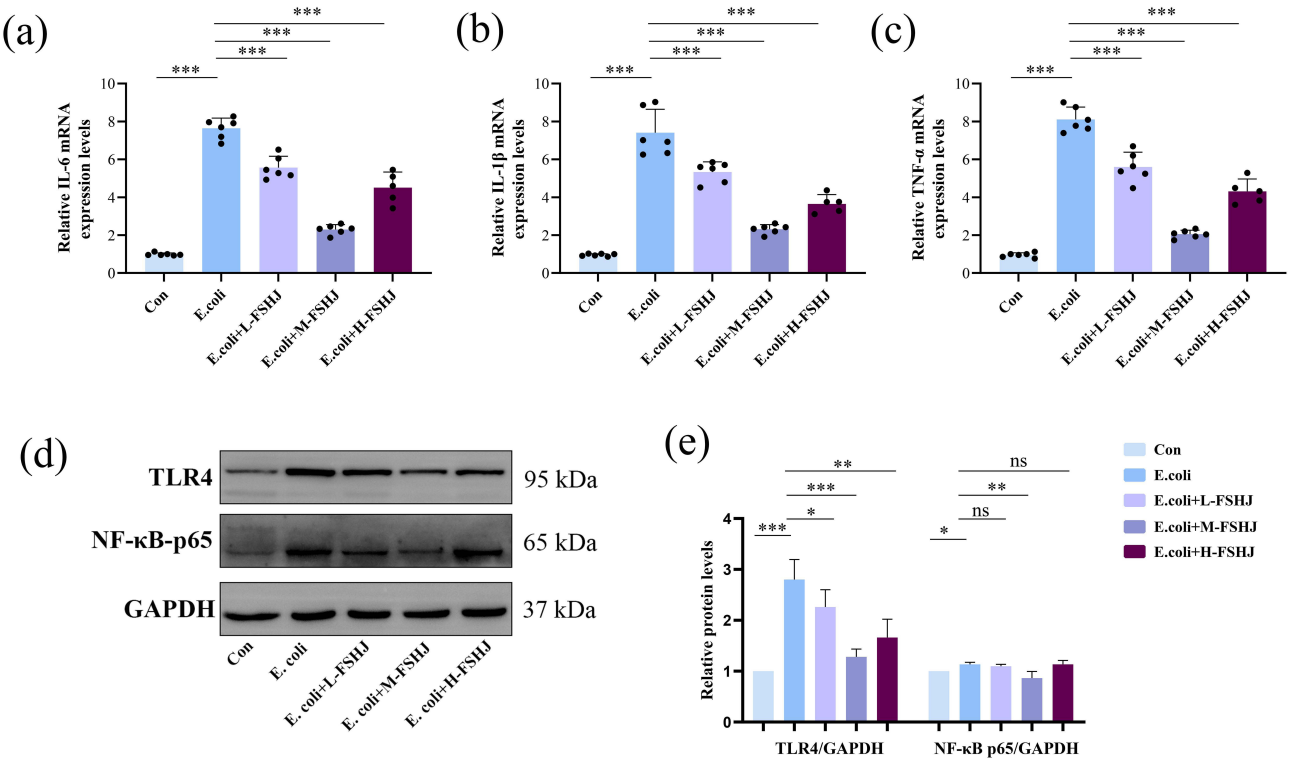

Figure 9 Experimental validation of FSHJ targets in sepsis-induced ARDS model. (**a–c**) Relative mRNA expression of IL-6, IL-1β, and TNF-α measured by qRT-PCR (n=5–6). (**d**) WB analysis of TLR4 and NF-κB p65 (n=3, Figure S1). (**e**) Quantitative analysis of WB results. *$P < 0.05$, **$P < 0.01$, ***$P < 0.001$. (**a–c** and **e**) were compared using one-way ANOVA with Fisher's LSD post hoc test.
Abbreviation: ns, not significant.

warranted to better assess the translational potential. Third, the sepsis model was induced by a single pathogen (*E. coli*). Given the polymicrobial nature of clinical sepsis, future studies employing polymicrobial infection models would enhance clinical relevance.

Conclusion

This study employed network pharmacology to identify primary drug components and potential targets of FSHJ in sepsis-induced ARDS treatment. Molecular docking and MDS validated these findings, confirming stable interactions between active components and key targets. Quercetin-3β-D-glucoside likely plays a significant therapeutic role. Subsequent in vivo experiments demonstrated that FSHJ alleviated pathological lung injury and pro-inflammatory cytokine production, potentially through the regulation of TLR4/NF-κB-mediated inflammatory signaling pathways.

Abbreviations

ALI, acute lung injury; ARDS, acute respiratory distress syndrome; *E. coli, Escherichia coli*; ELISA, Enzyme-Linked Immunosorbent Assay; FEL, free energy landscape; FSHJ, Fushuheji/Fusu agent; GO, Gene Ontology; KEGG, Kyoto Encyclopedia of Genes and Genomes; H&E, Hematoxylin and Eosin; HED, human equivalent dose; high-dose FSHJ, H-FSHJ; LC-MS, liquid chromatography-mass spectrometry; low-dose FSHJ, L-FSHJ; LPS, lipopolysaccharide; MCC, Maximal Clique Centrality; medium-dose FSHJ, M-FSHJ; MDS, molecular dynamics simulations; PCA, principal component analysis; PPI, protein-protein interaction; qRT-PCR, Quantitative Real-time PCR; Rg, radius of gyration; RMSD, root Mean Square Deviation; RMSF, root mean square fluctuation; SPF, specific pathogen-free; TCM, traditional Chinese medicine; TLRs, Toll-like receptors; W/D, wet-to-dry.

Data Sharing Statement

The data used to support our findings are included in the article, and information related to this study can be obtained from the corresponding author.

Ethics Statement

All animal experiments in this study were approved by the Ethics Committee of the Affiliated Hospital of Chengdu University of Traditional Chinese Medicine (approval number: 2024DL-034) and were conducted in adherence to the ARRIVE guidelines and the American Veterinary Medical Association guide for the care and use of animals.

Author Contributions

NJ: writing-original draft, methodology, formal analysis and investigation. XW: methodology, formal analysis and investigation, writing-review and editing. ML: formal analysis and investigation, software, writing-review and editing. JZ: writing-review and editing, visualization, funding acquisition. LH: writing-review and editing, methodology. GL: writing-review and editing, visualization. XZ: conceptualization, supervision, funding acquisition, data curation, writing-review and editing. PG: conceptualization, supervision, funding acquisition, resources, project administration, writing-review and editing.

All authors gave final approval of the version to be published; have agreed on the journal to which the article has been submitted; and agree to be accountable for all aspects of the work.

Funding

This research received financial support from The Sichuan Provincial Department of Science and Technology, the Central Guidance on Local Science and Technology Development Special Project (No. 2023ZYD0047), the General Program of the Natural Science Foundation of Sichuan Province (No. 25ZNSFSC0583), the Xinglin Scholar Program of Chengdu University of Traditional Chinese Medicine (No. MPRC2024012), and the Science and Technology Development Project of the Affiliated Hospital of Chengdu University of Traditional Chinese Medicine (No. 2025NSFCPY030), and the General Project of Sichuan Provincial Administration of Traditional Chinese Medicine (No. 25MSZX105).

Disclosure

The authors declare that there are no conflicts of interest.

References

1. Seymour CW, Liu VX, Iwashyna TJ, et al. Assessment of clinical criteria for sepsis: for the third international consensus definitions for sepsis and septic shock (Sepsis-3). *JAMA*. 2016;315(8):762–774. doi:10.1001/jama.2016.0288
2. Lin P, Gao R, Fang Z, et al. Precise nanodrug delivery systems with cell-specific targeting for ALI/ARDS treatment. *Int J Pharm*. 2023;644:123321. doi:10.1016/j.ijpharm.2023.123321
3. Auriemma CL, Zhuo H, Delucchi K, et al. Acute respiratory distress syndrome-attributable mortality in critically ill patients with sepsis. *Intensive Care Med*. 2020;46(6):1222–1231. doi:10.1007/s00134-020-06010-9
4. Jiao Y, Zhang T, Zhang C, et al. Exosomal miR-30d-5p of neutrophils induces M1 macrophage polarization and primes macrophage pyroptosis in sepsis-related acute lung injury. *Crit Care*. 2021;25(1):356. doi:10.1186/s13054-021-03775-3
5. Xu C, Zhang L, Xu S, et al. Neutrophil ALDH2 is a new therapeutic target for the effective treatment of sepsis-induced ARDS. *Cell Mol Immunol*. 2024;21(5):510–526. doi:10.1038/s41423-024-01146-w
6. Meyer NJ, Gattinoni L, Calfee CS. Acute respiratory distress syndrome. *Lancet*. 2021;398(10300):622–637. doi:10.1016/S0140-6736(21)00439-6
7. Bos LDJ, Ware LB. Acute respiratory distress syndrome: causes, pathophysiology, and phenotypes. *Lancet*. 2022;400(10358):1145–1156. doi:10.1016/S0140-6736(22)01485-4
8. Wang L, Tang Y, Tang J, et al. Endothelial cell-derived extracellular vesicles expressing surface VCAM1 promote sepsis-related acute lung injury by targeting and reprogramming monocytes. *J Extracell Vesicles*. 2024;13(3):e12423. doi:10.1002/jev2.12423
9. Xia D, Lu Z, Li S, et al. Development of an intelligent reactive oxygen species-responsive dual-drug delivery nanoplatform for enhanced precise therapy of acute lung injury. *Int J Nanomedicine*. 2024;19:2179–2197. doi:10.2147/IJN.S442727
10. Matthay MA, Zemans RL, Zimmerman GA, et al. Acute respiratory distress syndrome. *Nat Rev Dis Primers*. 2019;5(1):18. doi:10.1038/s41572-019-0069-0
11. Zhang N, Zhang H, Yu L, Fu Q. Advances in anti-inflammatory treatment of sepsis-associated acute respiratory distress syndrome. *Inflamm Res*. 2025;74(1):74. doi:10.1007/s00011-025-02043-2
12. Yin Z, Song R, Yu T, Fu Y, Ding Y, Nie H. Natural compounds regulate macrophage polarization and alleviate inflammation against ALI/ARDS. *Biomolecules*. 2025;15(2):192. doi:10.3390/biom15020192

13. Ding Z, Zhong R, Xia T, et al. Advances in research into the mechanisms of Chinese Materia Medica against acute lung injury. *Biomed Pharmacother*. 2020;122:109706. doi:10.1016/j.biopha.2019.109706
14. Liu Y, Wang X, Chen Y, et al. Pharmacological mechanisms of traditional Chinese medicine against acute lung injury: from active ingredients to herbal formulae. *Phytomedicine*. 2024;135:155562. doi:10.1016/j.phymed.2024.155562
15. Song Z, Kun-lan L, Lin Q, et al. A multi-center, prospective, randomized controlled trial of fusu agent combined with conventional western medicine in the treatment of acute respiratory distress syndrome. *Chin J Integr Trad Western Med*. 2022;42(3):298–304.
16. Gao P, Zhao Z, Zhang C, et al. The therapeutic effects of traditional Chinese medicine Fusu agent in LPS-induced acute lung injury model rats. *Drug Des Devel Ther*. 2018;12:3867–3878. doi:10.2147/DDDT.S181798
17. Chen J, Ding W, Zhang Z, et al. Shenfu injection targets the PI3K-AKT pathway to regulate autophagy and apoptosis in acute respiratory distress syndrome caused by sepsis. *Phytomedicine*. 2024;129:155627. doi:10.1016/j.phymed.2024.155627
18. Zhao L, Zhang H, Li N, et al. Network pharmacology, a promising approach to reveal the pharmacology mechanism of Chinese medicine formula. *J Ethnopharmacol*. 2023;309:116306. doi:10.1016/j.jep.2023.116306
19. Ferreira LG, Dos Santos RN, Oliva G, Andricopulo AD. Molecular docking and structure-based drug design strategies. *Molecules*. 2015;20 (7):13384–13421. doi:10.3390/molecules200713384
20. Kong X, Liu C, Zhang Z, et al. BATMAN-TCM 2.0: an enhanced integrative database for known and predicted interactions between traditional Chinese medicine ingredients and target proteins. *Nucleic Acids Res*. 2024;52(D1):D1110–D1120. doi:10.1093/nar/gkad926
21. Ru X, Chen S, Chen D, Shao Q, Shao W, Ye Q. Simulating the clinical manifestations and disease progression of human sepsis: a monobacterial injection approach for animal modeling. *Virulence*. 2024;15(1):2395835. doi:10.1080/21505594.2024.2395835
22. Uranga-Murillo I, Tapia E, Garzon-Tituana M, et al. Biological relevance of Granzymes A and K during *E. coli* sepsis. *Theranostics*. 2021;11 (20):9873–9883. doi:10.7150/thno.59418
23. Yang S, Yang Y, Wang F, et al. TREM2 dictates antibacterial defense and viability of bone marrow-derived macrophages during bacterial infection. *Am J Respir Cell Mol Biol*. 2021;65(2):176–188. doi:10.1165/rcmb.2020-0521OC
24. Zhou Y, Dong X, Xu D, Tang J, Cui Y. Therapeutic potential of traditional Chinese medicine for interstitial lung disease. *J Ethnopharmacol*. 2024;318(Pt A):116952. doi:10.1016/j.jep.2023.116952
25. Tang B, Xie L, Wang Y, et al. Exploratory research on the effective chemical basis of tanreqing injection for treating acute lung injury: in vivo, in vitro and in silico. *J Ethnopharmacol*. 2025;337(Pt 1):118780. doi:10.1016/j.jep.2024.118780
26. Wei-chao D, Juan C, Hao-yu L, et al. Mechanism of Xuebijing Injection in treatment of sepsis-associated ARDS based on network pharmacology and in vitro experiment. *China Journal of Chinese Materia Medica*. 2023;48(12):3345–3359. doi:10.19540/j.cnki.cjcmm.20230202.703
27. Cui J, Deng Y, Li X, et al. Herbal-based Xuebijing injection ameliorated vascular endothelial dysfunction via inhibiting ACLY/MYB/RIG-I axis in sepsis-associated lung injury. *Phytomedicine*. 2025;140:156573. doi:10.1016/j.phymed.2025.156573
28. Chen L, Song C, Zhang Y, et al. Quercetin protects against LPS-induced lung injury in mice via SIRT1-mediated suppression of PKM2 nuclear accumulation. *Eur J Pharmacol*. 2022;936:175352. doi:10.1016/j.ejphar.2022.175352
29. Ding W, Zhang W, Chen J, et al. Protective mechanism of quercetin in alleviating sepsis-related acute respiratory distress syndrome based on network pharmacology and in vitro experiments. *World J Emerg Med*. 2024;15(2):111–120. doi:10.5847/wjem.j.1920-8642.2024.030
30. Jiao Y, Li F, Chen M, et al. Pre-treatment with morphine prevents lipopolysaccharide-induced acute respiratory distress syndrome in rats via activation of opioid receptors. *Exp Cell Res*. 2022;418(1):113224. doi:10.1016/j.yexcr.2022.113224
31. Al-Kuraishy HM, Al-Gareeb AI, Negm WA, Alexiou A, Batiha GE. Ursolic acid and SARS-CoV-2 infection: a new horizon and perspective. *Inflammopharmacology*. 2022;30(5):1493–1501. doi:10.1007/s10787-022-01038-3
32. Liu Y, Zhou J, Luo Y, et al. Honokiol alleviates LPS-induced acute lung injury by inhibiting NLRP3 inflammasome-mediated pyroptosis via Nrf2 activation in vitro and in vivo. *Chin Med*. 2021;16(1):127. doi:10.1186/s13020-021-00541-z
33. Ge J, Yang H, Yu N, Lin S, Zeng Y. Wogonin alleviates sepsis-induced acute lung injury by modulating macrophage polarization through the SIRT1-FOXO1 pathways. *Tissue Cell*. 2024;88:102400. doi:10.1016/j.tice.2024.102400
34. Gao M, Zhu X, Gao X, et al. Kaempferol mitigates sepsis-induced acute lung injury by modulating the SphK1/S1P/S1PR1/MLC2 signaling pathway to restore the integrity of the pulmonary endothelial cell barrier. *Chem Biol Interact*. 2024;398:111085. doi:10.1016/j.cbi.2024.111085
35. Wang N, Tan S, Liu H, et al. SHP-1 alleviates acute liver injury caused by *Escherichia coli* sepsis through negatively regulating the canonical and non-canonical NFkappaB signaling pathways. *Int Immunopharmacol*. 2024;143(Pt 1):113371. doi:10.1016/j.intimp.2024.113371
36. Jiang J, Liu D, Wang Y, et al. Glaucocalyxin a protect liver function via inhibiting platelet over-activation during sepsis. *Phytomedicine*. 2022;100:154089. doi:10.1016/j.phymed.2022.154089
37. Zou P, Huang L, Li Y, et al. Phase-separated nano-antibiotics enhanced survival in multidrug-resistant *Escherichia coli* sepsis by precise periplasmic EcDsbA targeting. *Adv Mater*. 2024;36(44):e2407152. doi:10.1002/adma.202407152
38. Gong Z, Mao W, Zhao J, et al. TLR2 and NLRP3 orchestrate regulatory roles in *Escherichia coli* infection-induced septicemia in mouse models. *J Innate Immun*. 2024;16(1):513–528. doi:10.1159/000541819
39. Xu Y, Xin J, Sun Y, et al. Mechanisms of sepsis-induced acute lung injury and advancements of natural small molecules in its treatment. *Pharmaceuticals*. 2024;17(4):472. doi:10.3390/ph17040472
40. Wang Y, Li B, Zhang Y, Lu R, Wang Q, Gao Y. Qingfei Huoxue decoction and its active component narirutin alleviate LPS-induced acute lung injury by regulating tlr4/nf-kappab pathway mediated inflammation. *J Inflamm Res*. 2024;17:7503–7520. doi:10.2147/JIR.S480101
41. Wang W, Mu S, Yan D, Qin H, Zheng Z. Comprehending toll-like receptors: pivotal element in the pathogenesis of sepsis and its complications. *Front Immunol*. 2025;16:1591011. doi:10.3389/fimmu.2025.1591011
42. Nova Z, Skovierova H, Calkovska A. Alveolar-capillary membrane-related pulmonary cells as a target in endotoxin-induced acute lung injury. *Int J Mol Sci*. 2019;20(4). doi:10.3390/ijms20040831
43. Takeuchi O, Hoshino K, Kawai T, et al. Differential roles of TLR2 and TLR4 in recognition of gram-negative and gram-positive bacterial cell wall components. *Immunity*. 1999;11(4):443–451. doi:10.1016/S1074-7613(00)80119-3
44. Shen Y, Gong Z, Zhang S, et al. Besides TLR2 and TLR4, NLRP3 is also involved in regulating *Escherichia coli* infection-induced inflammatory responses in mice. *Int Immunopharmacol*. 2023;121:110556. doi:10.1016/j.intimp.2023.110556
45. Zhang C, Wang X, Wang C, et al. Qingwenzhike prescription alleviates acute lung injury induced by LPS via inhibiting TLR4/NF-κB pathway and NLRP3 inflammasome activation. *Front Pharmacol*. 2021;12:790072. doi:10.3389/fphar.2021.790072